JOURNAL OF CATALYSIS **161,** 659–666 (1996)
ARTICLE NO. 0228

Recovery of Bromine from Methyl Bromide Using Amorphous MnO_x Photocatalysts

Jung-Chou Lin,* Jie Chen,† Steven L. Suib,*,†,[1] Michael B. Cutlip,*,[1] and James D. Freihaut‡

*U-222, Department of Chemical Engineering, and †U-60, Department of Chemistry, University of Connecticut, Storrs, Connecticut 06269; and ‡United Technologies Research Center, Silver Lane, East Hartford, Connecticut 06108

Received October 23, 1995; revised March 20, 1996; accepted March 25, 1996

Amorphous MnO_x (AMO) has been prepared by the reaction of potassium permanganate and oxalic acid. Surface area measurements and pore size distribution analyses show that AMO has high surface (200 m^2/g) area and a microporus structure. Kinetic results indicate that methyl bromide degradation using AMO photocatalysts is due to a combination of thermocatalytic and photocatalytic reactions; however, the photocatalytic reaction is predominant. Detailed studies show that both molecular oxygen and bulk lattice oxygen of AMO can be involved in the oxidation of methyl bromide to carbon dioxide. Kinetic data, Auger analyses, and FTIR spectra suggest that both oxidation state changes of Mn and the presence of bromide adsorbed on the surface might lead to deactivation of the catalyst. According to mass balance calculations and analyses with potassium iodide solutions with starch, the final products are bromine, carbon dioxide, and water. The overall reaction for methyl bromide degradation under illumination using AMO photocatalyst can be expressed as

$$CH_3Br_{(g)} + \tfrac{7}{4}O_{2(g)} \rightarrow CO_{2(g)} + \tfrac{3}{2}H_2O_{(g)} + \tfrac{1}{2}Br_{2(g)}.$$

INTRODUCTION

The removal of hazardous organic compounds in air has become an important research topic over the past decade. The contamination of air with halogenated organic compounds presents a most serious environmental problem due to toxicity (1), carcinogenity (2), and destruction of the ozone layer (3, 4). The photocatalytic degradation of halogenated organics over semiconductors provides a promising solution to this environmental problem.

The heterogeneous photocatalytic degradation of halogenated compounds in aqueous solutions has been extensively investigated by Ollis and co-workers (5–10). Studies involving gas-phase heterogeneous photocatalysis are far fewer, but these reports have demonstrated that complete mineralization of halogenated organics with titanium dioxide photocatalysts can be achieved using molecular oxygen (11–14).

Manganese has been reported as an essential component in photosynthetic systems (15). Cao and Suib (16) prepared a variety of manganese oxide materials for the photooxidation of 2-propanol to acetone. Experimental results showed that amorphous MnO_x (AMO) is a highly efficient heterogeneous photocatalyst.

In this study, CH_3Br (believed to be an important ozone-depleting substance) was chosen as a model compound, and an AMO catalyst prepared by the reaction of potassium permanganate with oxalic acid was used as a photocatalyst (16). Experiments were carried out at various operating conditions. Results show that methyl bromide can be completely mineralized, i.e., degraded to Br_2, H_2O, and CO_2 by heterogeneous photocatalysis in a gas–solid system. A possible mechanism is proposed, and the deactivation of the catalyst has been investigated.

EXPERIMENTAL SECTION

Catalyst preparation. The AMO was prepared by the reaction of potassium permanganate and oxalic acid. The reaction was carried out by mixing solution A composed of 1.58 g potassium permanganate dissolved in 60 ml distilled deionized water (DDW) with solution B which was 2.26 g oxalic acid dissolved in 100 ml DDW. The resulting precipitated manganese oxide was washed with DDW and air-dried in an oven at 130°C. During the reaction, oxalic acid was oxidized to CO_2 and H_2O while the permanganate ion was reduced, precipitating out the AMO catalyst. Since the reaction was vigorous, CO_2 may have been encapsulated in the solid during particle growth. Upon drying, the escaping H_2O and CO_2 may have imparted a porous structure to the AMO.

Characterization. Brunauer, Emmett, and Teller (BET) surface area measurements (17) and pore size distribution analyses were done with an Ommisorp-100CX analyzer. Before undergoing physisorption experiments at 78 K with liquid nitrogen, 200-mg samples were loaded into the sample holder and outgassed at 150°C overnight to remove water and organics on the surface. Adsorption and

[1] To whom correspondence should be addressed.

0021-9517/96 $18.00

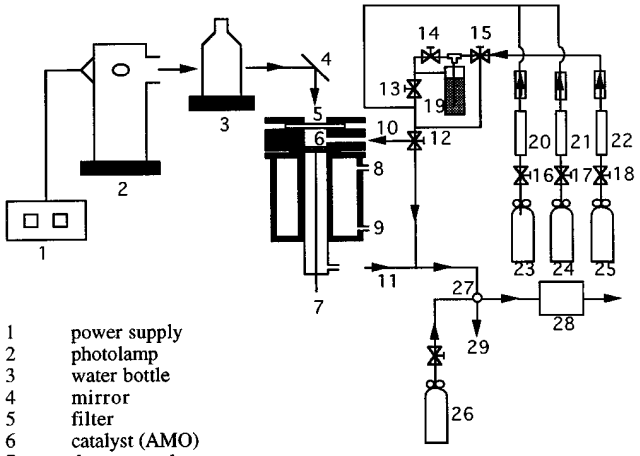

FIG. 1. Schematic diagram for the heterogeneous photocatalytic reactor system.

desorption isotherms were measured with the Omnisorp instrument. Surface areas based on the BET equation were calculated. Diffuse-reflectance ultraviolet-visible spectra for AMO were measured with a Hewlett Packard Diode Array 8452A spectrophotometer with a Labsphere RSA-HP-84 reflectance spectroscopy accessory. $BaSO_4$ was used as the standard. Auger electron spectroscopy analysis was done using a Perkin–Elmer PHI 610 Scanning Auger Microprobe (SAM). Data were collected under the following operating conditions: Beam voltage, 3 KV; beam current, 10 nA. Surface elemental analyses for fresh and spent amorphous MnO_x were conducted with SAM methods. FTIR spectroscopy in the far-IR range for amorphous MnO_x was conducted using a Nicolet Magna-IR 750 Spectrometer.

Catalysis. A schematic diagram for the heterogeneous photocatalytic reactor system is shown in Fig. 1. A xenon lamp which is similar to solar radiation was used as a light source, and a water bottle was used to remove IR radiation and thermal energy. Methyl bromide/N_2 mixtures blended with oxygen were fed into the stainless-steel reactor containing a thin layer of catalyst. In order to avoid homogeneous oxidation, a cutoff filter was used to exclude radiation of wavelengths less than 325 nm. Reactants and products were analyzed by gas chromatography (Perkin–Elmer Sigma 3) with a Porapak Q column using a thermal conductivity detector. Unless specifically mentioned, the current and voltage for the power supply were set at 40 A and 25 V respectively.

For the thermocatalytic experiments, AMO catalysts were loaded into a 3/8 in. o.d. tubular quartz reactor which was wrapped in heating tape connected to a temperature controller.

RESULTS

Figure 2 shows the XRD data for fresh AMO which is amorphous. No crystalline phase was observed for AMO after being used as a photocatalyst for the degradation of methyl bromide. AMO has a very small band gap energy

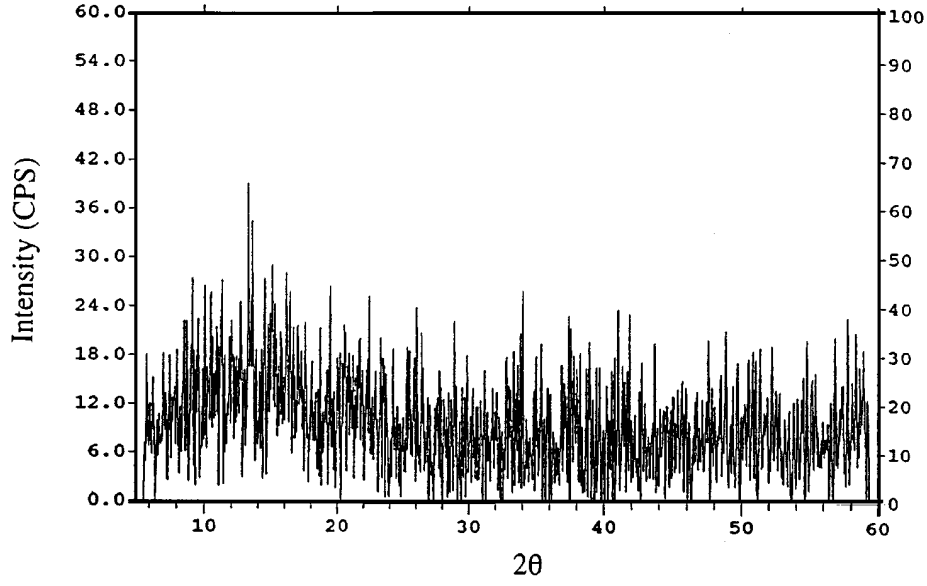

FIG. 2. XRD data for fresh AMO.

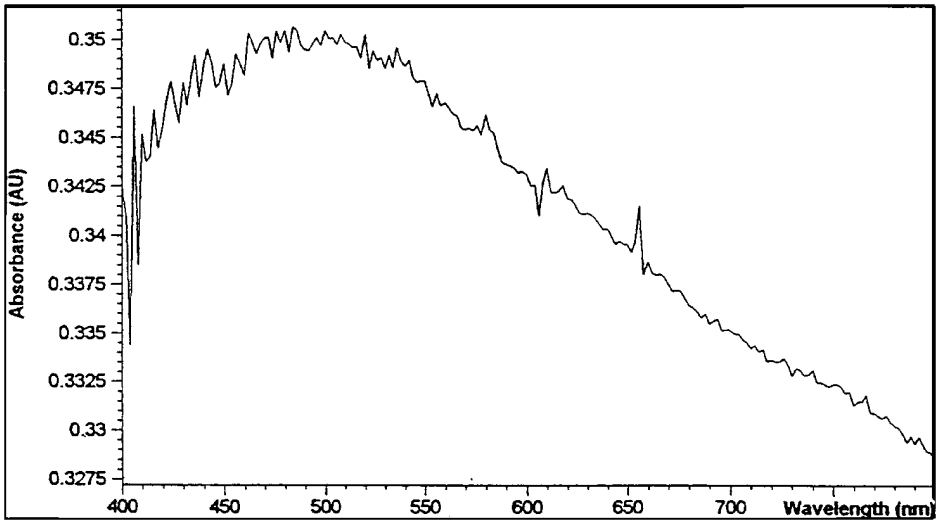

FIG. 3. Reflectance spectrum for AMO photocatalyst (blank, $BaSO_4$; $m_{MnO_x}/m_{BaSO_4} = 1/25$).

and can be activated by most of the solar spectrum as shown in Fig. 3. MnO_2 (p-type) has a small band gap energy which is 0.3 eV.

The surface area of AMO was about 200 ± 10 m^2/g. It is plausible that this catalyst is a porous material. Pore size distribution experiments were carried out by nitrogen adsorption followed by desorption. Results (Figs. 4 and 5) show that a micropore and dual mesopore distribution exists in this material. Micropore distribution analyses were based on the Horvath and Kawazoe method (18). Mesopore analyses were based on the BJH method (19) which involves the area of the pore walls and uses the Kelvin equation to correlate the partial pressure of nitrogen in equilibrium with the porous solid to the size of the pores where capillary condensation takes place.

During the heterogeneous photocatalytic experiments, the system temperature was always above ambient temperature (about 70°C). This was partly due to the radiation

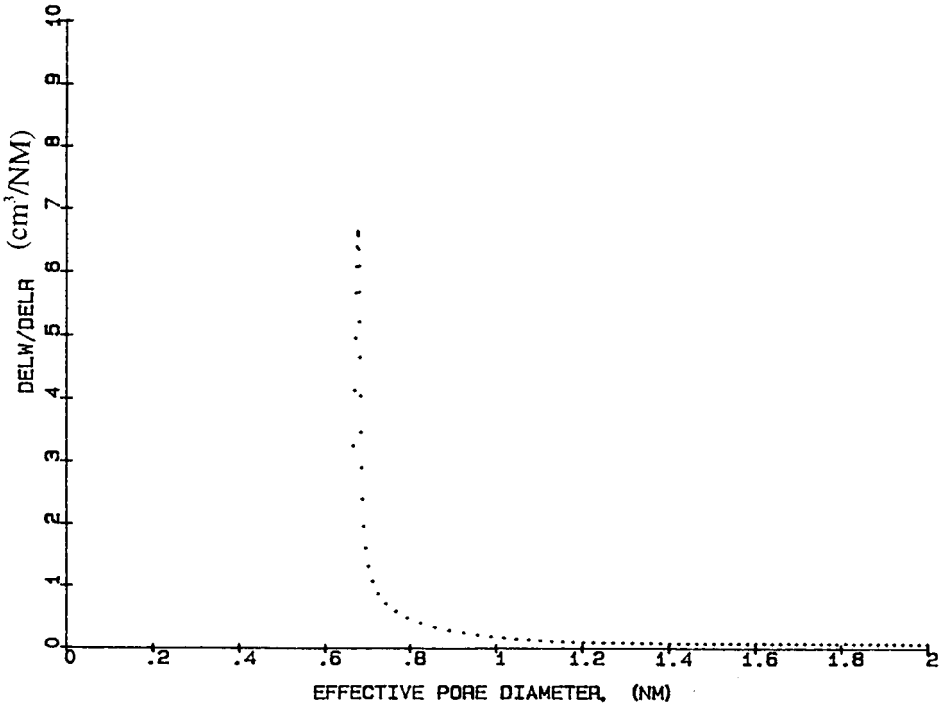

FIG. 4. Micropore size distribution for AMO.

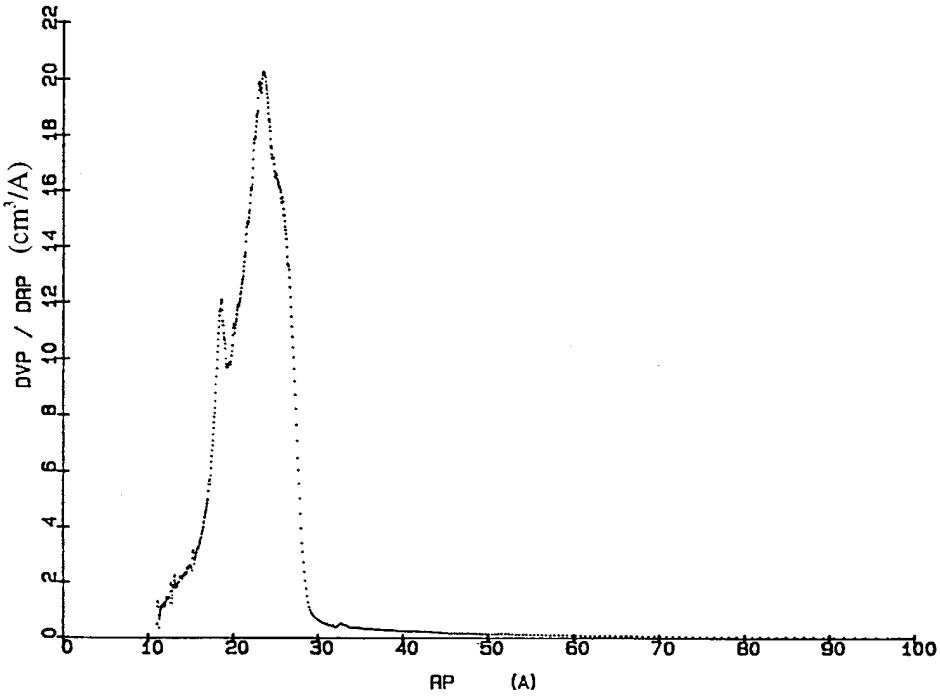

FIG. 5. Mesopore size distribution for AMO.

energy and partly due to the color of amorphous MnO_x (black) which can maximize the absorption and minimize back scattered radiation. Therefore, the thermodegradation of methyl bromide relative to the overall degradation was investigated. Figure 6 shows the thermocatalytic degradation of CH_3Br at 74°C which is approximately the system temperature of photocatalysis process using AMO catalyst. The resulting thermocatalytic conversion for methyl bromide degradation was about 10% and the recovery based on a carbon mass balance was about 70%. The percentage recovery based on the carbon was defined as

$$\text{Recovery} = \frac{\text{moles of } CO_2 \text{ produced}}{\text{moles of } CH_3Br \text{ consumed}} \times \% \qquad [1]$$

In order to determine which process (thermo or photo) dominates the degradation of methyl bromide, experiments were conducted with changing light intensity as shown in Fig. 7. The conversion for methyl bromide degradation was found to increase with increasing power intensity at

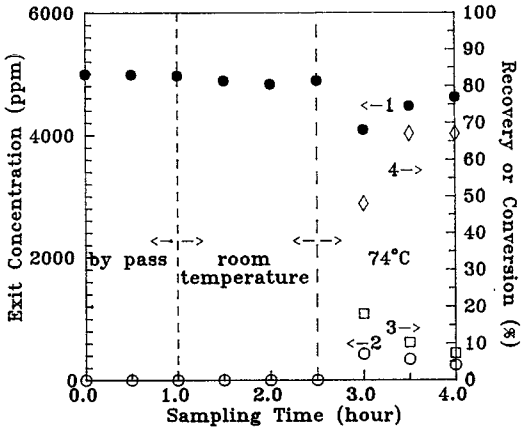

FIG. 6. Thermocatalytic degradation using AMO (inlet concentration, 4980 ppm; flow rate, 20 ml/min; system temperature, 74°C; oxygen mole fraction, 0.5; catalyst, 100 mg; 1, CH_3Br; 2, CO_2; 3, conversion; 4, recovery based on carbon).

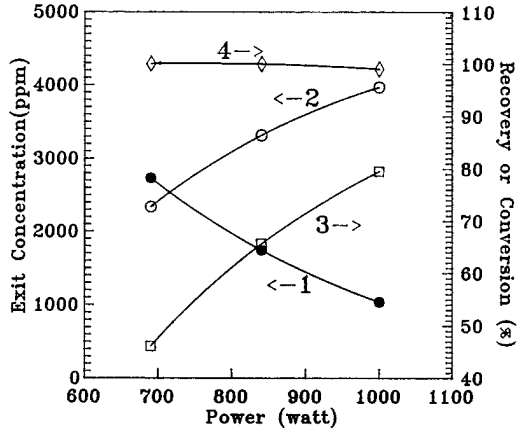

FIG. 7. Effect of power on methyl bromide degradation (inlet concentration, 5061 ppm; flow rate, 20 ml/min; system temperature, 60°C; oxygen mole fraction, 0.5; catalyst, 100 mg; 1, CH_3Br; 2, CO_2; 3, conversion; 4, recovery based on carbon).

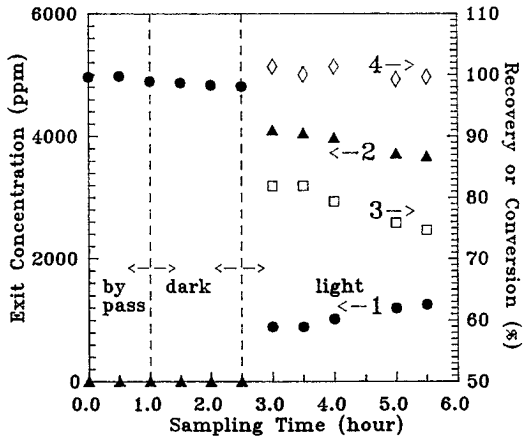

FIG. 8. Methyl bromide photocatalytic oxidation (inlet concentration, 4944 ppm; flow rate, 20 ml/min; system temperature, 70°C; oxygen mole fraction, 0.5; catalyst, 100 mg; 1, CH_3Br; 2, CO_2; 3, conversion; 4, recovery based on carbon).

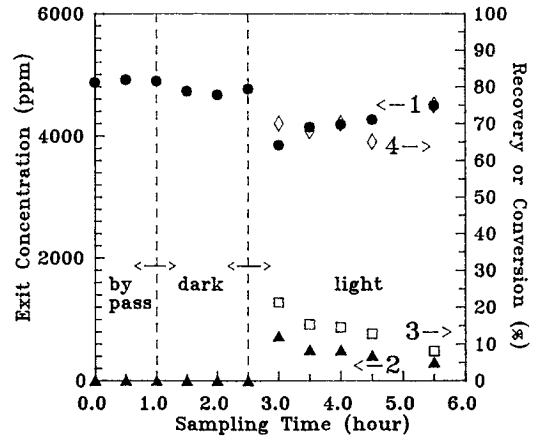

FIG. 9. Methyl bromide photocatalytic degradation under deoxygenating conditions (inlet concentration, 4892 ppm; flow rate, 20 ml/min; system tempeature, 77°C; catalyst, 100 mg; 1, CH_3Br; 2, CO_2; 3, conversion; 4, recovery based on carbon).

constant temperature. This is characteristic of a photocatalytic reaction.

Figure 8 shows that methyl bromide degraded under illumination. The conversion for photocatalytic degradation of methyl bromide was about 80% which was much higher than that for thermocatalytic degradation (less than 10%). Recovery based on carbon was about 100% which indicated that there was no coking on the surface of photocatalyst; and this was consistent with the Auger results in Table 1. There were negligible changes in the carbon concentration on the surfaces of fresh and spent catalysts which were tested under oxygenating conditions.

Methyl bromide was also photocatalytically degraded under deoxygenating conditions, and CO_2 formation was observed with gas chromatography methods as shown in Fig. 9. The conversion decreased with sampling time, and the recovery based on carbon was about 70%. Table 1 shows that carbon concentration on the surface increased for spent catalysts under deoxygenating conditions, and this can explain why recovery was about 70%.

Diffuse reflectance infrared spectra (Fig. 10) for fresh (a) and spent (b) AMO show that the structure of AMO was modified after the photocatalytic reaction.

A long-term experiment for methyl bromide degradation has been carried out (Fig. 11). Experimental results showed that the conversion of methyl bromide dropped rapidly at the early stage. However, reaction reached steady state at longer time on stream. No apparent deactivation is observed.

The turnover rates for methyl bromide degradation based on the assumption of continuous stirred tank reactor are summarized in Table 2. Turnover rates obtained under oxygenating conditions were about five times larger than those obtained under deoxygenating conditions. The color of the spent catalyst under oxygenating conditions remained black; however, the color of the spent catalyst under deoxygenating conditions changed from black to dark brown.

TABLE 1

Auger Analyses for Amorphous MnO_x

Spot	Br/Mn	K/Mn	C/Mn	O/Mn
		Fresh catalyst		
1	X	0.51	0.14	1.31
2	X	0.56	0.10	1.28
3	X	0.60	0.17	1.27
		Spent catalyst (oxygenating conditions)		
1	trace	0.37	0.11	1.15
2	trace	0.29	0.08	1.17
3	trace	0.33	0.09	1.18
		Spent catalyst (deoxygenating conditions)		
1	trace	0.89	0.32	1.21
2	trace	0.81	0.26	1.29
3	trace	0.78	0.29	1.25

DISCUSSION

Catalysis. For the thermodegradation of CH_3Br (Fig. 6), the conversion was low and the recovery was less than 100% which suggested that there should be some coking on the surface of AMO catalyst. When methyl bromide was photocatalytically degraded (Figs. 7 and 8), the conversion was high and increased with increasing applied power. The percentage recovery was 100%. These results indicate that methyl bromide degradation using AMO photocatalysts was due to a combination of thermocatalytic and photocatalytic reactions; however, the photocatalytic reaction was predominant.

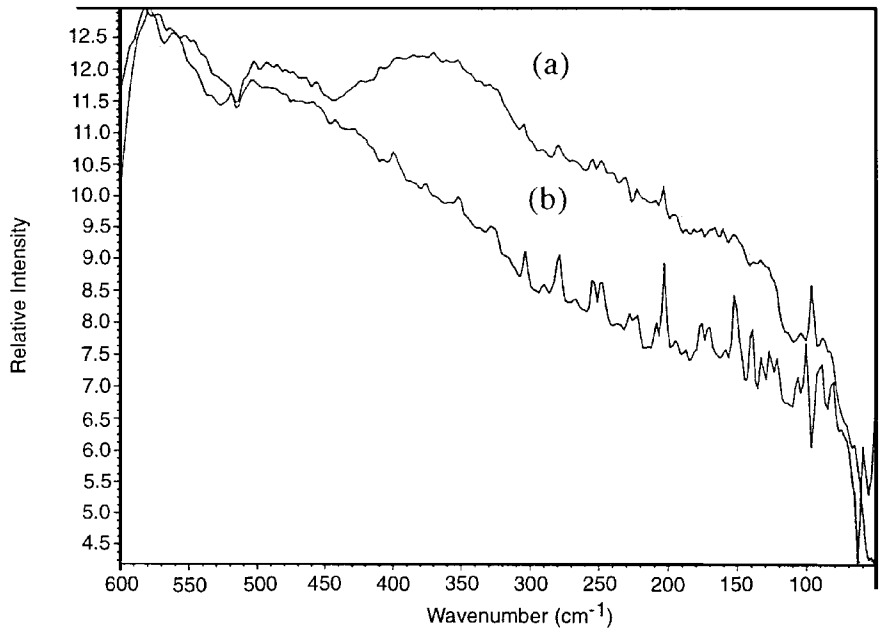

FIG. 10. Diffuse reflectance infrared spectra for AMO (a) fresh (b) spent.

Carbon dioxide has been identified as a final product.The source of oxygen for the methyl bromide oxidation may be molecular oxygen from the gas phase or bulk lattice oxygen of AMO. When the reaction was carried out under deoxygenating conditions (Fig. 9), low conversions and low recoveries were obtained. Table 1 shows negligible change in the O/Mn ratio for the fresh AMO and spent AMO under deoxygenating conditions; however, the observed increase in the K/Mn ratio indicates that the oxidation state of Mn has been reduced in order to maintain the charge balances on the surface of the spent catalyst. These results suggest that coking, decreasing oxygen concentrations, and bromide adsorbed on the active site of the catalyst surface (Table 1) might lead to the deactivation of the catalyst under deoxygenating conditions. However, a comparison (Table 2) between oxygenating conditions and deoxygenating conditions indicates that molecular oxygen from the gas phase is the main source of oxygen for the degradation of CH_3Br.

Although AMO shows promising results for the photocatalytic oxidation of CH_3Br such as high conversion and complete mineralization (1 mole of methyl bromide is converted to 1 mole of carbon dioxide based on a mass balance calculation) under oxygenating conditions, slow deactivation of AMO was observed during the photocatalytic process as shown in Fig. 8. Figure 9 shows that bulk lattice oxygen of AMO can be the source of oxygen for the oxidation of CH_3Br under deoxygenating conditions. Once bulk lattice oxygen of AMO is consumed by the reaction, oxygen concentrations on the surface may decrease, resulting in oxidation state changes in Mn. Figure 10 presents diffuse reflectance infrared spectra in the far-IR range for fresh and spent AMO (oxygenating conditions), respectively. Slow

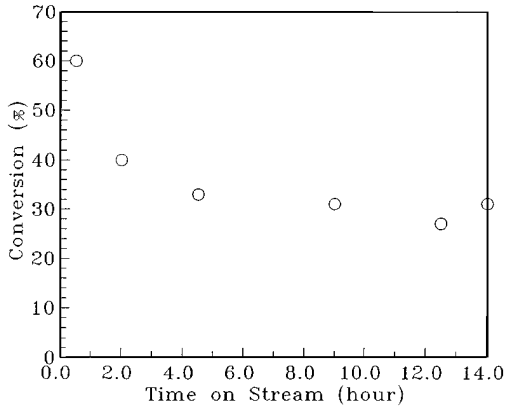

FIG. 11. Effect of time on stream on the conversion of methyl bromide degradation (inlet concentration, 5000 ppm; flow rate, 20 ml/min; system temperature, 68°C; catalyst, 100 mg; applied power, 800 W).

TABLE 2

Turnover Rate for the Degradation of Methyl Bromide[a]

Operating condition	Turnover rate[b]	Color of spent catalyst
Oxygenating	3.27×10^{-5}	Black
Deoxygenating	5.76×10^{-6}	Dark brown

[a] Inlet concentration of methyl bromide, 5000 ppm; O_2 concentration, 50%.

[b] Turnover rate, moles of CH_3Br consumed/g of catalyst·min.

consumption of oxygen on the surface might contribute to modification of fresh and spent catalysts and lead to slow deactivation of the catalyst. The reaction achieved steady state at longer time on stream. No apparent deactivation is observed. This suggests that material has reached a certain oxidation state and steady state desorption of bromine from the surface has occurred.

Overall reaction. Complete mineralization of methyl bromide in the presence of molecular oxygen can be achieved through the following overall reactions:

$$CH_3Br_{(g)} + \tfrac{3}{2}O_{2(g)} \rightarrow CO_{2(g)} + H_2O_{(g)} + HBr_{(g)} \quad [2]$$
$$\Delta G = -648520\ \text{J/mole}$$
$$CH_3Br_{(g)} + \tfrac{7}{4}O_{2(g)} \rightarrow CO_{2(g)} + \tfrac{3}{2}H_2O_{(g)} + \tfrac{1}{2}Br_{2(g)} \quad [3]$$
$$\Delta G = -708052\ \text{J/mole},$$

where ΔG is the Gibbs free energy of reaction. From the Gibbs free energy of reaction based on the ideal gas assumption, the formation of bromine (Eq. [3]) is thermodynamically favorable. Carbon dioxide and water have been observed by gas chromatography. The form of bromine product can be used to distinguish Eqs. [2] and [3]. Product distribution analysis for methyl bromide degradation was measured by FTIR. Peaks related to the HBr molecule were not found. Since CaF_2 windows were used for this IR cell, the Br_2 peak which is located in the far-IR range could not be observed.

The photoreactor was made of stainless steel. After reaction, the reactor wall was corroded by a red species. The red species was soluble in DDW and evaporated on exposure to air. Silver nitrate addition into the solution yielded a yellow precipitate indicating that there was bromide ion in the solution. After adding sodium hydroxide into the solution, a red precipitate formed. This suggests that the species in the water was $FeBr_3$. It is plausible that formation of $FeBr_3$ was due to the reaction between iron and Br_2 which appears to be the reaction product of methyl bromide degradation. Note from Eqs. [2] and [3] that Br_2 is favored thermodynamically.

Another glass-made photoreactor was built to rule out the possibility that steel reacts by corrosion. Reaction products were trapped in a dry ice trap and tested with KI solution with starch. These KI solutions with starch turned blue after mixing with the reaction products, suggesting that bromine was the reaction product for the degradation of methyl bromide.

Methyl bromide is believed to be an important ozone-depleting material. After degradation, bromine can be recovered by cold trap techniques and reused. HBr can be easily trapped by basic sodium hydroxide solution. However, when untreated methyl bromide is vented to the atmosphere, it will cause potential damage to the ozone layer.

Proposed mechanism. A plausible mechanism for the gas–solid photocatalytic degradation of CH_3Br is complicated. When illuminated with light of energy which is higher than the band gap, electrons and holes are formed in a semiconductor and are capable of initiating chemical reactions (20):

$$\text{solid} + h\nu \rightarrow h^+ + e^- + \text{solid}. \quad [4]$$

The formation of ·OH radicals can be achieved by the reaction of the valence band holes with either adsorbed H_2O or with surface OH^- groups:

$$h^+ + H_2O_{(ads)} \rightarrow \cdot OH + H^+ \quad [5]$$
$$OH^- + h^+ \rightarrow \cdot OH. \quad [6]$$

Kinetic results for methyl bromide degradation show that molecular oxygen from the gas phase is the primary source of the oxidation of methyl bromide to CO_2 and H_2O. Active oxygen species can form via the following steps (21–24):

$$O_{2(g)} \Leftrightarrow O_{2(ads)} \quad [7]$$
$$O_{2(ads)} + e^- \rightarrow \cdot O^-_{2(ads)}. \quad [8]$$

Of course, the active oxygen species can form by the reaction of bulk lattice oxygen with conduction band electrons:

$$O_{\text{lattice}} + e^- \rightarrow \cdot O^-. \quad [9]$$

Since adsorption is usually a necessary part of a catalytic process, methyl bromide might be adsorbed on the active site before reacting with active species on the surface:

$$CH_3Br_{(g)} \Leftrightarrow CH_3Br_{(ads)}. \quad [10]$$

For gas–solid reactions, oxygen species are abundant on the surface of the catalyst. Yate and co-workers (25, 26) investigated the photooxidation of methyl chloride on TiO_2 (110) single crystals and powdered surfaces. They reported that mineralization of methyl chloride occurs through oxygen adsorbed on defect sites not involving hydroxyl radicals. Although the detection of radicals by using EPR in our studies was not successful, experimental results for temperature programming desorption show that surface defects exist in this material (27). It is plausible that active oxygen species react with adsorbed methyl bromide and the formation of ·OH radicals might delay the electron-hole recombination process to increase the efficiency of reaction. The reactions between active oxygen species and methyl bromide are

$$2\cdot O^-_{2(ads)} + CH_3Br_{(ads)} + H^+ \rightarrow CO_{2(ads)} + 2H_2O_{(ads)} + Br^-_{(ads)} \quad [11]$$

or

$$6\cdot O^-_{(ads)} + CH_3Br_{(ads)} + H^+ \rightarrow CO_{2(ads)} + 4OH^- + Br^-_{(ads)}. \quad [12]$$

Based on the results of KI solution analyses and observed color changes in the reactor, Br_2 is the reaction product of methyl bromide degradation. The formation of Br_2 might occur via the reaction

$$MnO_2 + 2HBr_{(ads)} \rightarrow MnO + H_2O_{(ads)} + Br_{2(ads)}. \quad [13]$$

However, oxygen can reoxidize the MnO back to MnO_2. That may be why the color of spent catalysts was dark brown (MnO/Mn_2O_3) and black (MnO_2) for the deoxygenating and oxygenating operating conditions, respectively. The reaction for reoxidation of catalyst is

$$MnO + \tfrac{1}{2}O_2 \rightarrow MnO_2. \quad [14]$$

In the final step of the reaction sequence, the products of the surface reactions adsorbed on the surface are subsequently desorbed into the gas phase and can be identified by the GC. AMO is likely a mixed valent system of small amounts of Mn^{2+} and Mn^{3+} in Mn^{4+} before photocatalysis. In this regard, Eq. [14] represents partial oxidation of Mn^{2+} in the AMO.

CONCLUSIONS

Amorphous MnO_x has been prepared by the reaction of potassium permanganate and oxalic acid. Surface area and pore size distribution measurements have shown that this material has high surface area ($200 \pm 10\ m^2/g$) and a porous structure. Methyl bromide degradation processes using AMO photocatalysts were due to a combination of photocatalytic and thermal reactions; however, the photocatalytic reaction was predominant.

The oxygen source for the oxidation of methyl bromide to carbon dioxide may be molecular oxygen or bulk lattice oxygen from AMO (this is likely regenerated by molecular oxygen). Auger results showed that there was some coking on the surface of the spent catalyst for deoxygenating conditions. Bromide species which might poison the catalyst were observed on all spent catalysts. FTIR spectra showed that the catalyst had been modified after reaction, which might be due to consumption of surface oxygen. These observations suggest that oxidation state changes of Mn as well as bromide adsorbed on active sites might have been responsible for deactivation of these catalysts.

Bromine, carbon dioxide, and water were identified as final products. Methyl bromide can be degraded to bromine by photocatalytic processes using AMO photcatalysts, thereby allowing recovery of bromine.

ACKNOWLEDGMENTS

We thank the U.S. DOE, Office of Basic Energy Sciences, the EPA under the Pollution Prevention Research & Development Center, the Environmental Research Institute, University of Connecticut, and United Technologies Research Center, East Hartford, CT, for support of this work.

REFERENCES

1. Strier, M. P., *Environ. Sci. Technol.* **14**, 28 (1980).
2. Stiein, M. W., and Sansome, F. B., "Degradation of Chemical Carcinogens." Van Nostrand–Reinhold, New York, 1980.
3. Zurer, P., *CEW Chem. Eng. World* **November 14**, 29 (1994).
4. Solomon, S., *Nature* **347**, 347 (1990).
5. Pruden, A. L., and Ollis, D. F., *J. Catal.* **82**, 404 (1983).
6. Hsiao, C. Y., Lee, C. L., and Ollis, D. F., *J. Catal.* **82**, 418 (1983).
7. Ahmed, S., and Ollis, D. F., *Solar Energy* **32**(5), 597 (1984).
8. Ollis, D. F., Hsiao, C. Y., Budiman, L., and Lee, C. L., *J. Catal.* **88**, 89 (1984).
9. Nguyen, T., and Ollis, D. F., *J. Phys. Chem.* **88**, 3386 (1984).
10. Ollis, D. F., *Environ. Sci. Technol.* **19**(6), 480 (1985).
11. Dibble, L. A., and Raupp, G. B., *Catal. Lett.* **4**, 345 (1990).
12. Dibble, L. A., and Raupp, G. B., *Environ. Sci. Technol.* **26**, 492 (1992).
13. Yamazaki-Nishida, S., Nagano, K. J., Phillips, L. A., Cervera-March, S., and Anderson, M. A., *J. Photochem. Photobiol. A: Chem.* **70**, 95 (1993).
14. Nimlos, M. R., Jacoby, W. A., Blake, D. M., and Milne, T. A., *Environ. Sci. Technol.* **27**, 732 (1993).
15. Koulougliotis, D. H., Donald, J., and Brudvig, G. W., *J. Am. Chem. Soc.* **114**, 8322 (1992).
16. Cao, H., and Suib, S. L., *J. Am. Chem. Soc.* **116**, 5334 (1994).
17. Brunauer, B., Emmett, P. H., and Teller, E., *J. Am. Chem. Soc.* **60**, 309 (1938).
18. Horvath, G., and Kawazoe, K., *J. Chem. Eng. Jpn.* **16**(6), 470 (1983).
19. Barrett, E. P., Joyner, L. G., and Halenda, P. P., *J. Am. Chem. Soc.* **73**, 373 (1951).
20. Serpone, N., and Pelizzetti, E. (Eds.), "Photocatalysis." Wiley, New York, 1989.
21. Chon, H., and Pajeres, J., *J. Catal.* **14**, 257 (1969).
22. Formenti, N., Juillet, F., Meriaudeau, P., and Teichner, S. J., *Chemtech.* **1**, 680 (1971).
23. Herrmann, J. M., Disdier, J., Mozzanega, M. N., and Pichat, P., *J. Catal.* **60**, 369 (1979).
24. Courbon, H., Formenti, M., and Pichat, P., *J. Phys. Chem.* **81**, 550 (1977).
25. Wong, J. C. S., Linsebigler, A., Lu, G., Fan, J., and Yate, J. T., Jr., *J. Phys. Chem.* **99**, 335 (1995).
26. Lu, G., Linsebigler, A, and Yate, J. T., Jr., *J. Phys. Chem.* **99**, 7626 (1995).
27. Chen, J., Lin, J.-C., Yin, Y.-G., Suib, S. L., and Freihaut, J. D., manuscript in preparation.